Title

Archaeomagnetic results from Cambodia in Southeast Asia: Evidence for possible low-latitude flux expulsion

Journal

Proceedings of the National Academy of Sciences of the United States of America, 118(11)

ISSN

0027-8424

Authors

Cai, Shuhui
Doctor, Rashida
Tauxe, Lisa
et al.

Publication Date

2021-03-16

DOI

10.1073/pnas.2022490118

Peer reviewed

Archaeomagnetic results from Cambodia in Southeast Asia: Evidence for possible low-latitude flux expulsion

Shuhui Cai[a,b], Rashida Doctor[c], Lisa Tauxe[b,1], Mitch Hendrickson[d], Quan Hua[e], Stéphanie Leroy[f], and Kaseka Phon[g]

[a]State Key Laboratory of Lithospheric Evolution, Institute of Geology and Geophysics, Chinese Academy of Sciences, 100029 Beijing, China; [b]Scripps Institution of Oceanography, University of California San Diego, La Jolla, CA 92093; [c]Department of Earth and Environmental Sciences, University of Minnesota, Minneapolis, MN 55455; [d]Department of Anthropology, University of Illinois at Chicago, Chicago, IL 60607; [e]Australian Nuclear Science and Technology Organisation, Kirrawee DC, NSW 2232, Australia; [f]Laboratoire Archéomatériaux et Prévision de l'Altération–Institut de Recherche sur les Archéomatériaux, Nanosciences et Innovation pour les Matériaux la Biomédecine et l'Énergie, Commissariat à l'énergie atomique, CNRS, CEA Saclay, Université Paris-Saclay, Gif-sur-Yvette 91191, France; and [g]Institute of Humanities and Social Sciences, Royal Academy of Cambodia, Phnom Penh 12000, Cambodia

Contributed by Lisa Tauxe, January 7, 2021 (sent for review October 28, 2020; reviewed by Maria Luisa Osete and John Tarduno)

Extensive spatial and temporal distribution of high-quality data are essential for understanding regional and global behaviors of the geomagnetic field. We carried out chronological and archaeomagnetic studies at the Angkor-era iron-smelting site of Tonle Bak in Cambodia in Southeast Asia, an area with no data available to date. We recovered high-fidelity full-vector geomagnetic information from the 11th to 14th century for this region, which fill gaps in the global distribution of data and will significantly improve the global models. These results reveal a sharp directional change of the geomagnetic field between 1200 and 1300 CE, accompanied by an intensity dip between 1100 and 1300 CE. The fast geomagnetic variation recorded by our data provides evidence for the possible existence of low-latitude flux expulsion. Related discussions in this paper will inspire a new focus on detailed geomagnetic research in low-latitude areas around the equator, and exploration of related dynamic processes.

archaeology | archaeomagnetism | geomagnetic field behavior

The geomagnetic field is one of the Earth's fundamental properties, playing an important role in protecting the Earth from cosmic radiation (1) and more recently in human history for ground communication and navigation. The field is generated in the Earth's liquid outer core, and thus its evolution can provide us information regarding geodynamic processes in the Earth's deep interior (2–4). Archaeomagnetism, relying on heated artifacts from archaeological sites, has contributed significantly to understanding detailed features of the geomagnetic field during the Holocene and establishing regional (5–9) and global field models (10–12). However, the global distribution of the present archaeomagnetic data is patchy, with concentrations in some areas (e.g., Europe and the Levant) and major deficiencies in several other regions (e.g., the Southern Hemisphere and low-latitude areas in the Northern Hemisphere); the dearth in data hinders our understanding of the geomagnetic regional structures and precision of the global models. Southeast Asia is one of those areas with scarce archaeomagnetic data having only one known study of archaeodirectional data from Thailand (13). In this study, we conducted a full-vector archaeomagnetic investigation at the iron-smelting site of Tonle Bak located in north-central Cambodia. The archaeodirections will be the first from Cambodia and the archaeointensities will be the first from Southeast Asia, which will fill an important gap in the present global data distribution. Finally, our results will provide constraints for understanding detailed geomagnetic features as well as their interior dynamic processes.

Archaeological Background and Sampling

Archaeological studies identified the Phnom Dek region in north-central Cambodia as an important source of iron during the development of the Angkorian Khmer Empire, and particularly the major periods of expansion between the 11th and 13th centuries CE (Fig. 1*A*) (14–16). Located 135 km east of the Khmer capital of Angkor, this region contains over a dozen sites comprising up to 50 individual mounds consisting of stratigraphic layers with mixed technological debris from the smelting processes. The Tonle Bak site is situated 2 km south of Phnom Dek—literally the "Iron Mountain"—and was selected for excavation with the aim of documenting Angkorian iron technology and discovering evidence of lifestyles of the local smelting community. A total of seven trenches were excavated by the Industries of Angkor Project in 2017, uncovering considerable volumes of technical ceramics in the form of tuyères (air-delivery pipes), furnace fragments, and smelting slags (Fig. 1*B*). Most importantly, three furnaces were revealed on the top of Mound 2 (STB-02), which represent the first in situ furnaces discovered from the Angkor period. Each furnace is ∼2 m long and 1 m wide, with a slag pit on the west side. Multiple "ash tongues" leading into the slag pits (Furnace 1 in Trench 2, F1) and furnace bases (Furnace 2 in Trench 6, F2) were found that indicate reconstruction and reuse of the furnaces before being ultimately abandoned (15). F1 and F2 were restricted to furnace bases

Significance

The geomagnetic field contains information about interior dynamics of the Earth and is closely related to human beings on maintaining a habitable planet. Understanding variations of the field in the past, especially during the Holocene, is helpful for deciphering modern geomagnetic behaviors or even predicting future variations. Archaeomagnetism is efficient in recovering field information over the past millennia. However, the present data are not distributed evenly across the globe, limiting interpretation of the field features. We conducted an archaeomagnetic study on an iron-smelting site from Cambodia in Southeast Asia, an area currently devoid of data. The results will fill gaps in the present datasets and provide constraints for understanding specific geomagnetic features and their interior driving mechanism.

Author contributions: S.C., L.T., and M.H. designed research; S.C., R.D., L.T., M.H., and Q.H. performed research; S.C., Q.H., S.L., and K.P. contributed new reagents/analytic tools; S.C., R.D., Q.H., S.L., and K.P. analyzed data; L.T. edited and helped write the manuscript; and S.C. wrote the paper.

Reviewers: M.L.O., Universidad Complutense de Madrid; and J.T., University of Rochester.

The authors declare no competing interest.

[1]To whom correspondence may be addressed. Email: ltauxe@ucsd.edu.

This article contains supporting information online at https://www.pnas.org/lookup/suppl/doi:10.1073/pnas.2022490118/-/DCSupplemental.

Published March 8, 2021.

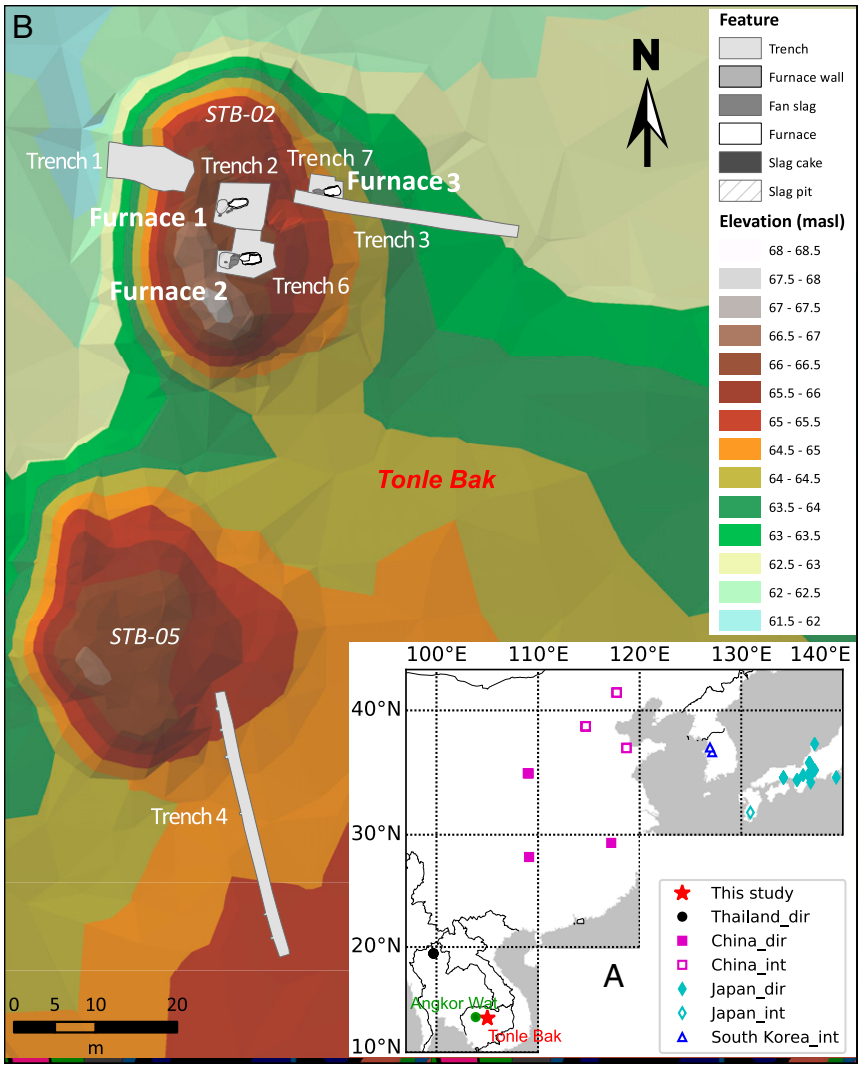

Fig. 1. (*A*) Site locations of Tonle Bak in this study (red star) and published archaeomagnetic data from Southeast-East Asia. Black circle, magenta square, cyan diamond, and blue triangle represent data from Thailand, China, Japan, and South Korea, respectively. Solid and open symbols represent directions and intensities, respectively. (*B*) Elevation map showing positions of the studied trenches and furnaces on the archaeological site.

while the furnace in Trench 7 (F3) also had partially preserved walls.

We collected oriented samples from the base of F1 and F2 (*SI Appendix*, Figs. S1*B* and S2*B*), and both the base and remaining walls from F3 (*SI Appendix*, Fig. S3*B*). Magnetic azimuth and dip were measured with a magnetic compass. Unoriented samples (tuyères, slags, and furnace fragments) were collected from the south wall of Trench 1 (T1S, *SI Appendix*, Fig. S4*A*), the south and west wall of Trench 3 (T3S and T3W, *SI Appendix*, Fig. S5 *A* and *B*), and the west wall of Trench 4 (T4W, *SI Appendix*, Fig. S6*A*). Charcoals (charred wood) were collected from all the furnaces and trench walls for radiocarbon dating. Positions of unoriented samples and charcoals through the walls were marked in cyan and red, respectively. Trenches 1–3 and 6–7 are all from STB-02 while Trench 4 is from Mound 5 (STB-05, Fig. 1*B*). Trench 5, located to ~100 m southeast of Mound 5, was not sampled.

Radiocarbon Dating

Radiocarbon dates were calibrated using the software Oxcal v4.3.2 (17) and a mixed calibration curve, 50% IntCal20 (18) and 50% SHCal20 (19), to account for a regional ^{14}C offset caused by atmospheric transport and mixing in tropical areas including Southeast Asia, which are influenced by monsoon circulation (19, 20). Calibrated dates from this site range from 1034 to 1391 CE. Radiocarbon results used in this study are listed in *SI Appendix*, Table S1, including both published dates (marked with stars) in Hendrickson et al. (15) and newly measured results. Multiple-sample radiocarbon plots for the three furnaces are shown in *SI Appendix*, Fig. S7 while those for the trench sections are shown in *SI Appendix*, Figs. S4*B*, S5*C*, and S6*B*, respectively.

Geomagnetic Direction

We collected eight (A–H), nine (A–I), and eight (A–H) oriented samples, respectively, from F1, F2, and F3 (*SI Appendix*, Figs. S1*B*, S2*B*, and S3*B*). Natural remanent magnetizations (NRMs) of the specimens are strong, ranging from 4.6 to 100 μAm^2 with the majority on the order of 10 μAm^2. All specimens except two show excellent demagnetization behavior, with one or two straight components in their directions after removing a limited viscous remanent magnetization. All the single-component specimens have high-quality statistical parameters: the number of points used in line fittings (n) $\geq$ 12; the deviation angle from the origin $\leq$ 3.5°, and the unanchored maximum angular

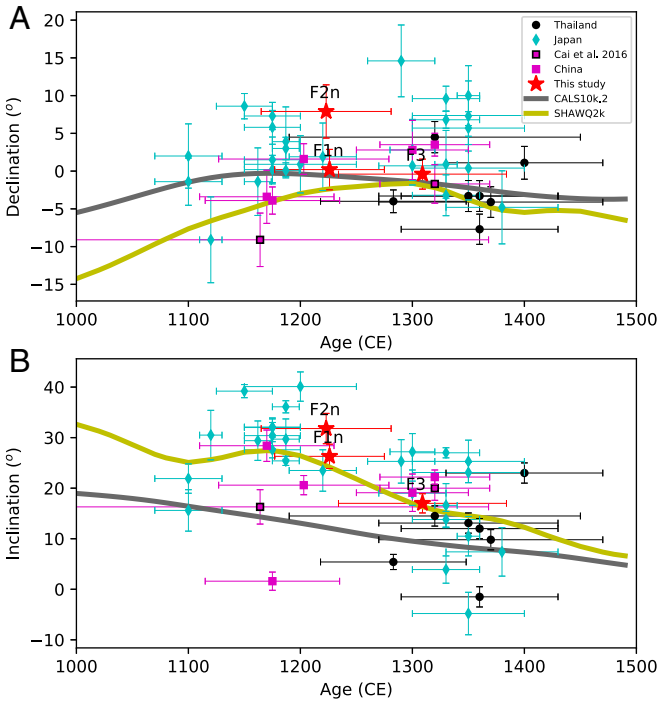

Fig. 2. Comparison of directional data from this study to those from Southeast-East Asia between 1100 and 1400 CE as well as to predictions at our studied site (13.29°N, 105.01°E) from global models CALS10k.2 (11) and SHAWQ2k (10). (*A* and *B*) Compilations of declinations and inclinations, respectively. All published data were relocated to our site.

deviation ≤ 3.6°. Statistical results on specimen and sample/site levels are listed in *SI Appendix*, Tables S2 and S3.

Samples from F1 can be divided into two groups (*SI Appendix*, Fig. S1 *A* and *B*) while those from F2 can be split into three groups according to their directional results (*SI Appendix*, Fig. S2 *A* and *B*). The groups sampled from the northern side of both furnaces show a single magnetic component (*SI Appendix*, Figs. S1*C* and S2*D*) while those from the southern sides show two-component behaviors (*SI Appendix*, Figs. S1*D* and S2*C*), and the latter records shallower directions than the former (*SI Appendix*, Figs. S1*A* and S2*A*). The two-component behaviors and shallower directions of the southern groups of the furnaces can be explained by disturbance of the southern furnace bases during cooling. The third group of F2, sampled from an area marked as possibly remagnetized on the eastern side of the furnace base, have directions that are single component but are distinct from other samples, and thus cannot be considered as reliable. Samples collected from F3 record single-component (*SI Appendix*, Fig. S3 *C* and *D*) and consistent directions (*SI Appendix*, Fig. S3*A*). These are all from the furnace wall (*SI Appendix*, Fig. S3*B*), since the only sample from the base broke during cutting, and were apparently not disturbed after cooling. Detailed discussions about reliability of these directions can be found in *SI Appendix*, *Part 1*. Finally, we conclude that the single-component directions recorded by samples from the northern sides of the furnace bases of F1 and F2 as well as all directions from F3 are likely primary and represent geomagnetic directions when the furnaces were last used before being abandoned.

Age of each furnace is constrained by the maximum range of radiocarbon dates from that furnace (*SI Appendix*, Fig. S7).

Geomagnetic Intensity

Sister specimens to the oriented samples collected from the furnaces as well as unoriented samples taken from the trenches (T1, T3, and T4) were selected for paleointensity experiments. A total of 360 specimens from 66 samples were measured. Only 13 out of 66 samples (58 out of 360 specimens) yielded acceptable results, with low success rates of ∼20 and ∼16% on sample and specimen level, respectively. Representative Arai plots (21) of accepted specimens with the sample pictures are shown in *SI Appendix*, Fig. S8. Quite a few specimens, especially slags, behaved poorly, failing either because of alteration or nonlinear behavior. Among the 13 successful samples, only two are slags while the others are tuyères and furnace fragments. Specimens from oriented samples also behave poorly, mostly showing curved Arai plots, with only one sample (T7-F3-Ei) that passed our criteria (*SI Appendix*, Fig. S8*H*). Another successful sample (T2-F1-2i) from the furnace is a piece of unoriented red fragment (*SI Appendix*, Fig. S8*G*). The rest of the successful samples are from the trenches. Results of the accepted specimens and samples are listed in *SI Appendix*, Tables S5 and S6, respectively. Paleointensities recovered from this site vary from ∼27 to ∼44 μT.

We combine the radiocarbon dating, stratigraphy, and paleointensity information to constrain ages of samples that passed our criteria in the paleointensity experiments from the trench sections. Detailed discussions can be found in *SI Appendix*, *Part 2*. Ages of the two successful samples from F1 and F3 are constrained by the age of each furnace.

Sharp Change of Geomagnetic Direction

We compiled published geomagnetic directional data between 1100 and 1400 CE from East and Southeast Asia (Figs. 1*A* and 2), including both recently published (22) and older data from the GEOMAGIA50.v3.3 database (23) from Japan, China, and Thailand. Data from the database were selected with 95% confidence limit (α_{95}) ≤ 5°, and only those with an age uncertainty were included. All the accepted data were relocated to the studied site (13.29°N, 105.01°E) through the conversion via virtual geomagnetic pole method (24). Results from this study are compared to the relocated published data and predictions of global models at our site (Fig. 2). Declinations of our new data fit the model CALS10k.2 (11) and SHAWQ2k (10), with the exception of F2n, which deviates eastward. Inclinations approximate to predictions from SHAWQ2k but deviate significantly from CALS10k.2, which is probably because the latter was smoothed greatly and did not include data published between 2016 and 2019. Our new data agree with the published data generally, showing a westward swing in declination and shallowing of inclination between 1200 and 1300 CE. We projected our new directions and the published data from adjacent area of Thailand (∼880 km from our site) around 1200–1300 CE on an equal area plot for a better view of the variation trajectory of the geomagnetic field (Fig. 3). Declination of the field moves

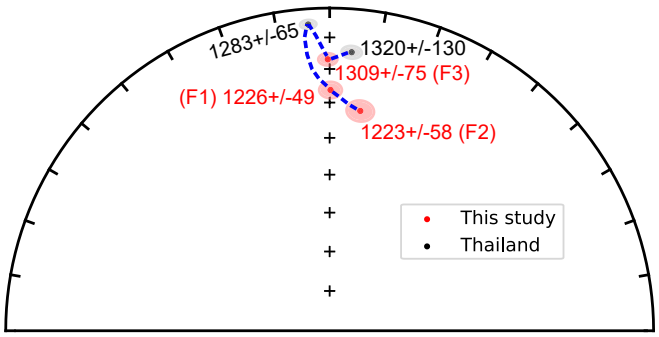

Fig. 3. Equal area projections of directions from this study (red) and Thailand (black) around 1200–1300 CE. Their α_{95} intervals are shown as ellipses. Numbers on the plot are ages and their errors in CE.

westward from ~8° to ~−4° while inclination becomes shallower from ~30° to ~5° between ~1220 and ~1280 CE. This is followed by a sharp turn at ~1280 CE, and after that the declination moves eastward to ~5° while the inclination recovers to ~15° until ~1320 CE. The average angular variation rates calculated with angular differences and mean ages between 1223 and 1283 CE and 1283 and 1309 CE are ~0.48° and ~0.47°/y while the low boundaries of angular variation rates calculated with maximum age intervals for these two time periods are ~0.16° and ~0.07°/y, respectively. The average angular variation rate of the modern field at the studied site Tonle Bak between 1900 and 2000 is ~0.05°/y. Even the minimum variation rates are larger than the average rate of the modern field, demonstrating that the direction of the geomagnetic field changed rapidly between 1200 and 1300 CE. This result provides evidence for the recent inference from the observational field model and geodynamo simulations that rapid directional changes are prone to happen in low-latitude areas and are likely related to the movement of reversed flux patches across the core surface (25). Our studied site is at low latitude and is indeed proximal to a low-intensity anomaly, probably associated with reverse flux patches at core–mantle boundary (3), between ~1200 and 1300 CE (*SI Appendix*, Fig. S9 *B* and *C*) and outside the patches between 1900 and 2000 CE (*SI Appendix*, Fig. S9 *I* and *J*). It is worth mentioning that variations of the field direction are constrained by the very few available data in this area presently, and could be updated by new reliable data in the future.

Dip in Geomagnetic Intensity and Implications for Low-Latitude Flux Expulsion

The geomagnetic intensities obtained from Tonle Bak vary from ~27 to ~44 μT (~64–106 ZAm^2) between 1100 and 1300 CE (Fig. 4*A*). Our results deviate from predictions of the global model CALS10k.2 significantly, and fit better to SHAWQ2K and the regional reference curve of ArchInt_China.2 (6). Prediction of the global model SHAWQ2K is consistent with the regional model of ArchInt_China.2 and fits better to the new data because it was calculated with volcanic and archaeomagnetic data and includes new published data in recent years, and thus can capture certain details of the field variation. However, our data record much lower values between ~1200 and 1300 CE (Fig. 4*B*). Combined with data published recently from China (5, 26), South Korea (27) and Japan (28), our data outline a U-shape variation of the field strength with a dip between ~1200 and 1300 CE, coincident with the sharp change of the field direction.

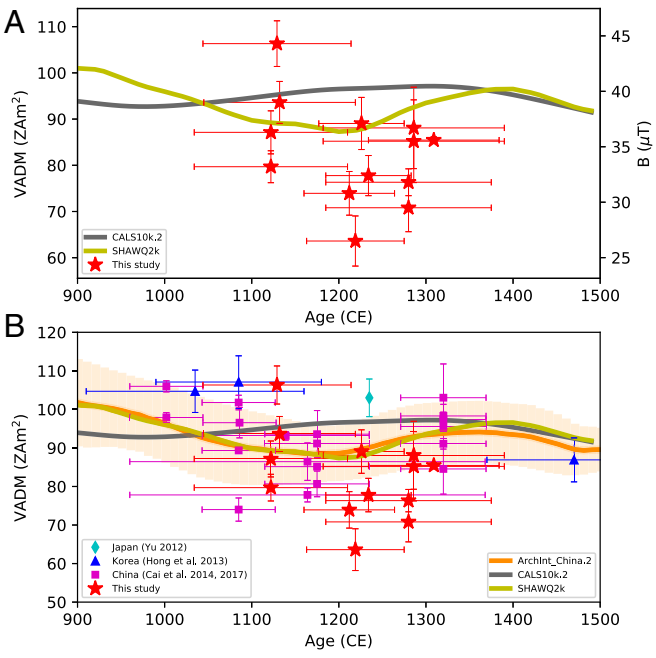

Fig. 4. (*A*) Paleointensities in μT and associated virtual axial dipole moments of our data. (*B*) Comparisons of our paleointensities to data published recently from China (5, 26), South Korea (27), and Japan (28). Gray and yellow lines are predictions at our studied site (13.29°N, 105.01°E) from global models CALS10k.2 (11) and SHAWQ2k (10), respectively. Orange line is the Chinese archaeointensity reference curve (ArchInt_China.2) (6).

Tarduno et al. (3) reported a geomagnetic anomaly with sharp directional change and intensity drop at ~1300 CE in southern Africa. They attributed this anomaly to a reversal of flux caused by flux expulsion in the core–mantle boundary, which is related to unusual topography, such as the African large low-shear velocity province (29), beneath the site. They further infer that the studied site in southern Africa may have been a steady area for flux expulsion and accumulation and reconnection of the generated reversal flux patches may trigger geomagnetic reversals. Our results record a similar geomagnetic anomaly over the approximate time frame in Southeast Asia, which is probably driven by reversed flux at the core–mantle boundary as well. The global model SHAWQ2k predicts a large geomagnetic intensity anomaly across the equatorial latitudes (Fig. 5*A*). Both our studied site and the mentioned site in southern Africa are located in the range of this anomaly, which allows us to speculate that the predicted large equatorial geomagnetic anomaly (EGA) probably represents an average of multiple low geomagnetic anomalies, considering the smoothing effect when calculating the model, driven by a series of reversal flux in this area. To further inspect this hypothesis, we compiled data from the latitudinal range related to the EGA, including Africa (Fig. 5*B*), South America (Fig. 5*D*), and Southwest Pacific (Fig. 5*E*), during the time period of 1000–1500 CE and compared them to the Southeast–East Asian compilation (Fig. 5*C*). The results of these areas show similar trends with dips in the field strength between 1100 and 1400 CE, varying in amplitudes and timing of minima. Results of the compilations confirm our speculation that the EGA embodies multiple low geomagnetic anomalies, probably controlled by reversed flux patches at the core–mantle boundary. One possible scenario to explain this phenomenon is the existence of flux expulsion over this low-latitude area.

The EGA spans the latitudinal area near the equator and a large longitudinal area across South America, the Atlantic, Africa, the Indian Ocean, and Southeast Asia, with its east side extending to the west Pacific area. It has been moving around with various sizes and shapes in this area since 1100 CE or earlier (*SI Appendix*, Fig. S9): combined as one large anomaly until ~1500 CE, started to separate into two patches at ~1500–1600 CE, and split completely at ~1900 CE. One of the two patches moved eastward to the Pacific Ocean, while the other patch shifted westward and centered between South America and eastern Africa, forming the well-known South Atlantic Anomaly (SAA). Shrinking, expanding, and shifting of the EGA could be controlled by reversed flux patches generated from the mentioned low-latitude flux expulsion at the core–mantle boundary, and thus reflect dynamic processes in the Earth's interior. This raises a few issues to be considered. For instance, what is the interior driving mechanism of the low-latitude flux expulsion? Are they generated from multiple local small structures (e.g., vortices or eddies) concurrently, or the generated reversal patches propagate among areas? If the former, it means the structure of the core–mantle beneath this area is probably complex, so that flux expulsion happens commonly. In the latter case, we should observe differences in time of the geomagnetic features among various areas. Although the present datasets display general variation trends, they cannot satisfy requirement of discussing the concurrent or propagating issue either in

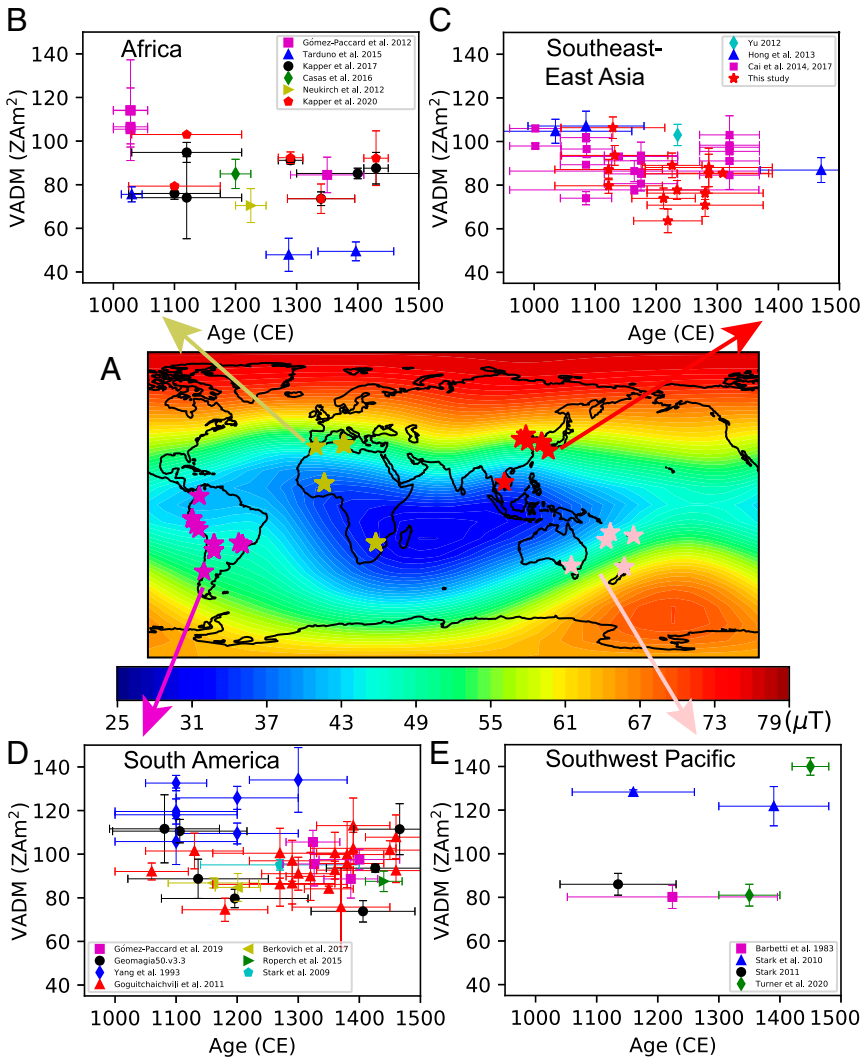

Fig. 5. Compilations of data from the latitudinal range related to the EGA during time period of 1000–1500 CE. (*A*) Global distribution of total field intensity at the Earth's surface predicted from SHAWQ2k. (*B–E*) Compilations of data from Africa (3, 7, 42–45), Southeast-East Asia (5, 26–28), South America (46–51), and Southwest Pacific (52–55).

quantity or in age precision. Studies have suggested that the SAA is a recurring feature (3, 10, 30). How about the other geomagnetic anomalies? Will these reversed flux patches reconnect and evolve to a geomagnetic reversal? High-quality data with low age uncertainty, e.g., decades, from certain areas, e.g., the discussed low latitudes around the equator, and time spans are necessary for clarifying these issues. Besides, numerical simulation about the interior structure and flow movement is also essential for understanding these features and informing their future development.

Implications of Geomagnetic Results for Archaeological Context

Archaeomagnetic results can provide us information for understanding the archaeological background in some cases. In this study, paleointensities from T1S fall into two groups and thus provide independent evidence that supports the radiocarbon dating results indicating the mound was formed over two distinct periods.

Dates for F1 and F2 are not distinguishable within the calibration error while their directions are close but significantly different since their α_{95} intervals do not overlap (Fig. 3). This indicates these two furnaces were used at a similar time period yet not exactly simultaneously, at least having distinguishable times of abandonment. Considering the pattern of the geomagnetic field variations in Fig. 2, our data fit the trend better if F2 is older than F1, which is also supported by variation trajectory of the field in Fig. 3. Therefore, by assuming that the variation trend of the geomagnetic field outlined by the compiled data are reliable, we can conclude that F2 was abandoned some time earlier than F1.

Summary

We recovered geomagnetic directions and intensities with precise age constraints and stringent selection criteria from the 11th to 14th century from the Angkorian iron-smelting site of Tonle Bak in Cambodia, Southeast Asia. These results from an area with no archaeomagnetic data to date improve distributions of the global dataset, and thus provide the benefit of understanding detailed structures of the geomagnetic field and the driving mechanisms. Our results revealed a sharp directional change of the geomagnetic field between 1200 and 1300 CE, with higher angular variation rate than the modern field. This is accompanied by an intensity dip between 1100 and 1300 CE. The fast

variation recovered by our data provides observational evidence for the recent simulation results from Davies and Constable (25) demonstrating that rapid directional changes are prone to occur in low latitudes when the field strength is weaker. Our results, combined with compiled data from areas related to the large equatorial geomagnetic anomaly, provide evidence for possible existence of the low-latitude flux expulsion. Evolution of these geomagnetic features should be paid special attention when deciphering related interior geodynamic processes and predicting future variations of the field.

Materials and Methods

Dating. Radiocarbon dating was conducted at the Australian Nuclear Science and Technology Organization (ANSTO). The charcoal samples were pretreated using the standard acid–alkali–acid method to remove all possible carbon contaminations. The pretreated samples were then combusted to CO_2 and converted to graphite using the Fe/H_2 method (31). Accelerator mass spectrometry radiocarbon analysis was carried out using the STAR facility at ANSTO (32) with a typical 1-sigma uncertainty of 0.25–0.3%.

Thermal Demagnetization. The oriented samples were cut into 2-cm cubic specimens in the laboratory. The sample F3-F was broken during processing and did not allow any oriented specimens. About three to six specimens were selected from each of the samples for stepwise thermal demagnetization measurements. A total of 86 specimens were measured. Specimens were thermally demagnetized in a laboratory-built oven with residual field less than 10 nT at the paleomagnetic laboratory in Scripps Institution of Oceanography (SIO), University of California San Diego. The specimens were heated in 50 °C intervals from 100 to 250 °C, 25 °C intervals until 500 °C, and 20 °C intervals at higher temperatures until nearly demagnetized. NRM and remaining remanence after each thermal step were measured by a 2G cryogenic magnetometer.

We analyzed the data with the 'Demag GUI' function incorporated in the PmagPy software (33) and calculated the direction of characteristic remanent magnetization for each specimen following the method of principal component analysis (34). Unanchored line interpretation without origin was used. Mean directions were calculated with Fisher statistics (35).

Paleointensity. Samples were crushed into chips and selected fresh specimens were fixed in 12-mm-diameter glass tubes with microfiber paper and potassium-silicate glue. The same laboratory-built oven for thermal demagnetization was used for paleointensity experiments, whose cooling time from high temperature to room temperature is ~30–45 min and ~12 h with the fan on and off, respectively. Measurements were made on the 2G magnetometer. Experiments were conducted in the magnetically shielded room at SIO.

The IZZI method (36) was used to determine the intensity of the ancient field with a partial thermal remanent magnetization (pTRM) check (37) inserted every other step. After paleointensity experiment, results of successful specimens were corrected for the effect of anisotropy of TRM (38) and cooling rate (39). Data were selected with the same criteria as used in Cai et al. (6), which is a modified version of the CCRIT criteria (40). Data were analyzed with the Thellier GUI function (41) incorporated in the PmagPy software package (33). Detailed description about experimental procedures and data selection criteria can be found in *SI Appendix*, *Part 3*.

Data Availability. Paleomagnetic data have been deposited in the Magnetics Information Consortium (MagIC) database (DOI: 10.7288/V4/MAGIC/17101).

ACKNOWLEDGMENTS. We thank the Ministry of Culture and Fine Arts of Cambodia for their collaboration and permission to undertake excavations at Tonle Bak. Additionally, we thank Justin Higa for performing part of the measurements. This work was supported by National Nature Science Foundation of China Grants 41888101, 41974077, and 41621004, NSF Grants EAR1550850 (to M.H.) and EAR1547263 (to L.T.), and CAS Grant GJHZ1776. S.C. acknowledges support from the Chinese Academy of Sciences (CAS) Pioneer Hundred Talents Program and the Key Research Program of the Institute of Geology and Geophysics (CAS Grant IGGCAS-201904).

1. J. A. Tarduno, E. G. Blackman, E. E. Mamajek, Detecting the oldest geodynamo and attendant shielding from the solar wind: Implications for habitability. *Phys. Earth Planet. Inter.* **233**, 68–87 (2014).
2. J. Aubert, C. C. Finlay, A. Fournier, Bottom-up control of geomagnetic secular variation by the Earth's inner core. *Nature* **502**, 219–223 (2013).
3. J. A. Tarduno *et al*., Antiquity of the South Atlantic Anomaly and evidence for top-down control on the geodynamo. *Nat. Commun.* **6**, 7865 (2015).
4. A. Nilsson, N. Suttie, M. Korte, R. Holme, M. Hill, Persistent westward drift of the geomagnetic field at the core–mantle boundary linked to recurrent high-latitude weak/reverse flux patches. *Geophys. J. Int.* **222**, 1423–1432 (2020).
5. S. Cai *et al*., Archaeointensity results spanning the past 6 kiloyears from eastern China and implications for extreme behaviors of the geomagnetic field. *Proc. Natl. Acad. Sci. U.S.A.* **114**, 39–44 (2017).
6. S. Cai *et al*., High-fidelity archeointensity results for the Late Neolithic period from central China. *Geophys. Res. Lett.* **47**, e2020GL087625 (2020).
7. L. Kapper *et al*., Novel insights on the geomagnetic field in West Africa from a new intensity reference curve (0-2000 AD). *Sci. Rep.* **10**, 1121 (2020).
8. A. Goguitchaichvili *et al*., Last three millennia Earth's Magnetic field strength in Mesoamerica and southern United States: Implications in geomagnetism and archaeology. *Phys. Earth Planet. Inter.* **279**, 79–91 (2018).
9. M. Gómez-Paccard *et al*., New constraints on the most significant paleointensity change in Western Europe over the last two millennia. A non-dipolar origin? *Earth Planet. Sci. Lett.* **454**, 55–64 (2016).
10. S. A. Campuzano, M. Gómez-Paccard, F. J. Pavón-Carrasco, M. L. Osete, Emergence and evolution of the South Atlantic Anomaly revealed by the new paleomagnetic reconstruction SHAWQ2k. *Earth Planet. Sci. Lett.* **512**, 17–26 (2019).
11. C. Constable, M. Korte, S. Panovska, Persistent high paleosecular variation activity in southern hemisphere for at least 10 000 years. *Earth Planet. Sci. Lett.* **453**, 78–86 (2016).
12. F. J. Pavón-Carrasco, M. L. Osete, J. M. Torta, A. De Santis, A geomagnetic field model for the Holocene based on archaeomagnetic and lava flow data. *Earth Planet. Sci. Lett.* **388**, 98–109 (2014).
13. M. Barbetti, D. Hein, Palaeomagnetism and high-resolution dating of ceramic kilns in Thailand: A progress report. *World Archaeol.* **21**, 51–70 (1989).
14. M. Hendrickson, S. Leroy, Q. Hua, K. Phon, V. Voeun, Smelting in the shadow of the iron mountain: Preliminary field investigation of the industrial landscape around Phnom Dek, Cambodia (ninth to twentieth centuries A.D.). *Asian Perspect.* **56**, 55–91 (2017).
15. M. Hendrickson *et al*., Forging empire: Angkorian iron smelting, community and ritual practice at Tonle Bak. *Antiquity* **93**, 1586–1606 (2019).
16. M. Hendrickson, S. Leroy, Sparks and needles: Seeking catalysts of state expansions, a case study of technological interaction at Angkor, Cambodia (9th to 13th centuries CE). *J. Anthropol. Archaeol.* **57**, 10.1016/j.jaa.2019.101141 (2020).
17. C. Bronk Ramsey, Methods for summarizing radiocarbon datasets. *Radiocarbon* **59**, 1809–1833 (2017).
18. P. J. Reimer *et al*., The IntCal20 Northern Hemisphere radiocarbon age calibration curve (0-55 cal kBP). *Radiocarbon* **62**, 725–757 (2020).
19. A. G. Hogg *et al*., SHCal20 Southern Hemisphere calibration, 0-55,000 years cal BP. *Radiocarbon* **62**, 759–778 (2020).
20. Q. Hua, M. Barbetti, Influence of atmospheric circulation on regional $^{14}CO_2$ differences. *J. Geophys. Res.*, 10.1029/2006JD007898 (2007).
21. T. Nagata, Y. Arai, K. Momose, Secular variation of the geomagnetic total force during the last 5000 years. *J. Geophys. Res.* **68**, 5277–5281 (1963).
22. S. Cai *et al*., New archaeomagnetic direction results from China and their constraints on palaeosecular variation of the geomagnetic field in Eastern Asia. *Geophys. J. Int.* **207**, 1332–1342 (2016).
23. M. C. Brown *et al*., GEOMAGIA50.v3: 1. General structure and modifications to the archeological and volcanic database. *Earth Planets Space*, 10.1186/s40623-015-0232-0 (2015).
24. M. Noel, C. M. Batt, A method for correcting geographically separated remanence directions for the purpose of archaeomagnetic dating. *Geophys. J. Int.* **102**, 753–756 (1990).
25. C. J. Davies, C. G. Constable, Rapid geomagnetic changes inferred from Earth observations and numerical simulations. *Nat. Commun.* **11**, 3371 (2020).
26. S. Cai *et al*., Geomagnetic intensity variations for the past 8 kyr: New archaeointensity results from Eastern China. *Earth Planet. Sci. Lett.* **392**, 217–229 (2014).
27. H. Hong *et al*., Globally strong geomagnetic field intensity circa 3000 years ago. *Earth Planet. Sci. Lett.* **383**, 142–152 (2013).
28. Y. Yu, High-fidelity paleointensity determination from historic volcanoes in Japan. *J. Geophys. Res.* **117**, B08101 (2012).
29. E. J. Garnero, A. K. McNamara, S.-H. Shim, Continent-sized anomalous zones with low seismic velocity at the base of Earth's mantle. *Nat. Geosci.* **9**, 481–489 (2016).
30. R. I. F. Trindade *et al*., Speleothem record of geomagnetic South Atlantic anomaly recurrence. *Proc. Natl. Acad. Sci. U.S.A.* **115**, 13198–13203 (2018).
31. Q. Hua *et al*., Progress in radiocarbon target preparation at the ANTARES AMS Centre. *Radiocarbon* **43**, 275–282 (2001).
32. D. Fink *et al*., The ANTARES AMS facility at ANSTO. *Nucl. Instrum. Methods Phys. Res. B* **223-224**, 109–115 (2004).
33. L. Tauxe *et al*., PmagPy: Software package for paleomagnetic data analysis and a bridge to the magnetics information Consortium (MagIC) database. *Geochem. Geophys. Geosyst.* **17**, 2450–2463 (2016).
34. J. Kirschvink, The least-squares line and plane and the analysis of palaeomagnetic data. *Geophys. J. R. Astron. Soc.* **62**, 699–718 (1980).
35. R. A. Fisher, Dispersion on a sphere. *Proc. R. Soc. A* **217**, 295–305 (1953).
36. Y. Yu, L. Tauxe, A. Genevey, Toward an optimal geomagnetic field intensity determination technique. *Geochem. Geophys. Geosyst.*, 10.1029/2003GC000630 (2004).

37. R. S. Coe, S. Grommé, E. A. Mankinen, Geomagnetic paleointensities from radiocarbon-dated lava flows on Hawaii and the question of the Pacific nondipole low. *J. Geophys. Res. Solid Earth* **83**, 1740–1756 (1978).
38. R. J. Veitch, I. G. Hedley, J. J. Wagner, An investigation of the intensity of the geomagnetic field during Roman times using magnetically anisotropic bricks and tiles. *Arch. Sci.* **37**, 359–373 (1984).
39. A. Genevey, Y. Gallet, Intensity of the geomagnetic field in western Europe over the past 2000 years: New data from French ancient pottery. *J. Geophys. Res.*, 10.1029/2001JB000701 (2002).
40. G. Cromwell, L. Tauxe, H. Staudigel, H. Ron, Paleointensity estimates from historic and modern Hawaiian lava flows using glassy basalt as a primary source material. *Phys. Earth Planet. Inter.* **241**, 44–56 (2015).
41. R. Shaar, L. Tauxe, G. U. I. Thellier, An integrated tool for analyzing paleointensity data from Thellier-type experiments. *Geochem. Geophys. Geosyst.* **14**, 677–692 (2013).
42. M. Gómez-Paccard *et al*., Archaeomagnetic and rock magnetic study of six kilns from North Africa (Tunisia and Morocco). *Geophys. J. Int.* **189**, 169–186 (2012).
43. L. Kapper *et al*., Reconstructing the geomagnetic field in West Africa: First absolute intensity results from Burkina Faso. *Sci. Rep.* **7**, 45225 (2017).
44. L. Casas *et al*., New archaeomagnetic data from Tunisia: Dating of two kilns and new archaeointensities from three ceramic artifacts. *Geoarchaeology* **31**, 564–576 (2016).
45. L. P. Neukirch *et al*., An archeomagnetic analysis of burnt grain bin floors from ca. 1200 to 1250 AD Iron-Age South Africa. *Phys. Earth Planet. Inter.* **190-191**, 71–79 (2012).
46. M. Gómez-Paccard *et al*., New archeointensity data from NW Argentina (1300–1500 CE). *Phys. Earth Planet. Inter.* **286**, 92–100 (2019).
47. S. Yang, J. Shaw, T. C. Rolph, Archaeointensity studies of Peruvian pottery-from 1200 B.C. to 1800 A.D. *J. Geomag. Geoelectr.* **45**, 1193–1207 (1993).
48. A. Goguitchaichvili, C. Greco, J. Morales, Geomagnetic field intensity behavior in South America between 400 AD and 1800 AD: First archeointensity results from Argentina. *Phys. Earth Planet. Inter.* **186**, 191–197 (2011).
49. C. S. Berkovich, A. Goguitchaichvili, G. A. Peña León, J. Morales, The first archaeointensity results from Colombia: Pre-Hispanic sites along Magdalena river (Honda-Tolima and Puerto Bogotá-Cundinamarca). *Arqueol. Iberoam.* **33**, 10–17 (2017).
50. P. Roperch, A. Chauvin, L. E. Lara, H. Moreno, Secular variation of the Earth's magnetic field and application to paleomagnetic dating of historical lava flows in Chile. *Phys. Earth Planet. Inter.* **242**, 65–78 (2015).
51. F. Stark, R. Leonhardt, J. W. Fassbinder, M. Reindel, "The field of sherds: Reconstructing geomagnetic field variations from Peruvian potsherds" in *New Technologies for Archaeology*, M. Reindel, G. A. Wagner, Eds. 2009), pp. 103–116.
52. M. Barbetti, M. W. McElhinny, D. J. Edwards, P. W. Schmidt, "Archeomagnetic results from Australia" in *Geomagnetism of Baked Clays and Recent Sediments*, K. M. Creer, P. Tucholka, C. E. Barton, Eds. (Elsevier, Amsterdam, 1983), pp. 173–175, 324 pp.
53. F. Stark, J. Cassidy, M. J. Hill, J. Shaw, P. Sheppard, Establishing a first archaeointensity record for the SW Pacific. *Earth Planet. Sci. Lett.* **298**, 113–124 (2010).
54. F. Stark, "Secular variation of the Earth's magnetic field in the south west Pacific," Doctoral dissertation, University of Liverpool, UK (2011).
55. G. M. Turner, R. Kinger, B. McFadgen, M. Gevers, The first archaeointensity records from New Zealand: Evidence for a fifteenth century AD archaeomagnetic 'spike' in the SW pacific region? *Geol. Soc. Lond. Spec. Publ.*, 10.1144/sp497-2019-71 (2020).